International Journal of Bioprinting

RESEARCH ARTICLE

High-throughput fabrication of cell spheroids with 3D acoustic assembly devices

Tingkuan Miao[1†], Keke Chen[1,2†*], Xiaoyun Wei[1,2], Beisi Huang[1], Yuecheng Qian[1], Ling Wang[1,2*], Mingen Xu[1,2*]

[1]School of Automation, Hangzhou Dianzi University, Hangzhou 310018, China

[2]Key Laboratory of Medical Information and 3D Bioprinting of Zhejiang Province, Hangzhou Dianzi University, Hangzhou 310018, China

Abstract

Acoustic cell assembly devices are applied in cell spheroid fabrication attributed to their rapid, label-free and low-cell damage production of size-uniform spheroids. However, the spheroids yield and production efficiency are still insufficient to meet the requirements of several biomedical applications, especially those that require large quantities of cell spheroids, such as high-throughput screening, macro-scale tissue fabrication, and tissue repair. Here, we developed a novel 3D acoustic cell assembly device combined with a gelatin methacrylamide (GelMA) hydrogels for the high-throughput fabrication of cell spheroids. The acoustic device employs three orthogonal piezoelectric transducers that can generate three orthogonal standing bulk acoustic waves to create a 3D dot-array (25 × 25 × 22) of levitated acoustic nodes, enabling large-scale fabrication of cell aggregates (>13,000 per operation). The GelMA hydrogel serves as a supporting scaffold to preserve the structure of cell aggregates after the withdrawal of acoustic fields. As a result, mostly cell aggregates (>90%) mature into spheroids maintaining good cell viability. We further applied these acoustically assembled spheroids to drug testing to explore their potency in drug response. In conclusion, this 3D acoustic cell assembly device may pave the way for the scale-up fabrication of cell spheroids or even organoids, to enable flexible application in various biomedical applications, such as high-throughput screening, disease modeling, tissue engineering, and regenerative medicine.

Keywords: Acoustic cell assembly; Levitated acoustic nodes; Cell spheroids; Drug screening; High-throughput fabrication

[†]These authors contributed equally to this work.

***Corresponding authors:**
Keke Chen
(kkchen@hdu.edu.cn)

Ling Wang
(lingw@hdu.edu.cn)

Mingen Xu
(xumingen@hdu.edu.cn)

Citation: Miao T, Chen K, Wei X, *et al*., 2023, High-throughput fabrication of cell spheroids with 3D acoustic assembly devices. *Int J Bioprint*.
https://doi.org/10.18063/ijb.733

Received: February 20, 2023
Accepted: March 17, 2023
Published Online: April 17, 2023

1. Introduction

During the last decades, cell spheroids as advantageous models were used in various biomedicine studies, such as drug screening[1], disease modeling[2], tissue engineering, and regenerative medicine[3]. Compared to commonly two-dimensional (2D) monolayer cultures, tumor spheroids represent better *in vivo* histological and biological characteristics, such as three-dimensional (3D) distribution of nutrients, metabolites and oxygen, as well as complex interactions of cells and extracellular matrix[4], making their drug responses similar to those found *in vivo*[5-7]. More recently, cell spheroids as building blocks promise to bring tissue engineering to next level[8-10]. Instead of

individual cells as building blocks, the high cell density of spheroids coupled with self-synthesized extracellular matrix endow fabricated tissues with faster maturation and better functionality[11-14]. With these merits, more advances based on spheroids have been potentially developed in several fields of high-throughput screening[15], precision medicine[16,17], and complex large tissue fabrication[18], however, which puts forward higher criteria on cell spheroids with identical morphology and physiology as well as in sufficient quantity[19,20].

To date, many technologies have been developed to fabricate cell spheroids[21-23]. A hanging drop was frequently used, due to easy handling and user-friendliness[24,25]. Based on gravity force, cells in small drops would settle and aggregate at the bottom of the drop, and eventually formed spheroids. This method generates spheroids in uniform size, but it is labor-intensive, time-consuming, and low-throughput. Several commercially available methods, including spinner flask[26], rotary cell culture system[27], and low-attachment microplate[28], enable mass production. However, the shear stress may induce cell damage and poor size uniformity, and the microplate (*e.g.*, AggreWell) is not cost-effective. Other engineering methods, such as microfluidic[29-31], electric[32], and magnetic-assisted[33] assembly of spheroids, are capable of size control, whereas they have some shortcomings, such as complex device fabrication, medium modification, and/or cell labeling. For example, cells were labeled by magnetic nanoparticles or suspended in a paramagnetic medium for robust assembly by magnetic forces, which might adversely affect cell growth or physiology[34,35]. Therefore, taking into account the problems with the above methods, more advanced spheroid-formation approaches are highly desirable to fulfill the requirements, including simplicity, ease of operation, biocompatibility, uniformity in size, and large-scale production.

As an alternative solution, acoustic assembly technique may generate better cell spheroids because it enables excellent biocompatibility and provides label-free manipulation of cells[36-38]. Commonly, this technique employs acoustic waves to create standing acoustic fields that have spatial distribution of periodic array of acoustic nodes (ANs)[39-41]. In these fields, suspension cells in culture medium are moved to the nearby ANs and assembled into cell aggregates under the action of acoustic radiation force, thereby rapidly generating cell spheroids with uniform size[42]. So far, several designs of acoustic assembly device have been developed for the generation of spheroids. For instance, standing surface acoustic waves (SAWs) were combined with a disposable capillary or multi-PDMS channels to form a 1D (1 × 30) or 2D (200 × 60) dot-array of ANs, respectively[38,43]. The latter can assemble more than 12,000 uniform cell aggregates per operation. One problem of this system is that the structure of the loosely assembled cell aggregates was easily damaged during the process of transferring from the channel to the Petri dish, resulting in a low maturation efficiency of spheroids. Besides, the ANs of SAW-based device was located near the substrate surface, limiting the capability to create more ANs to further improve the yield of aggregates[36,44]. In contrast, bulk acoustic waves (BAWs)-based devices enabled the formation of standing wave fields throughout the chamber[40,45,46]. Jeger-Madiot presented a multi-trap acoustic levitation device to create a 1D (1 × 30) plane-array of ANs, where cells can be levitated into multiple paralleled layers vertically and self-organized from cell sheets to cell spheroids[47]. Cai *et al.* used two standing BAWs to create a 2D (10 × 10) column-array of ANs so that 100 cell aggregates can be generated horizontally[48]. Despite this, the number of ANs produced by existing BAW-based devices was still small for mass production of cell spheroids. Nevertheless, these above works inspired us to investigate whether the 2D column-array of ANs in BAWs-based devices could be divided into 3D dot-array of ANs, when applying an acoustic levitation field, to create 10 × 10 × 30 dot-array of ANs so as to enable further improvement of yield of cell aggregates or spheroids by more than an order of magnitude.

Herein, we developed a 3D acoustic assembly device based on BAWs capable of creating a 3D dot-array of levitated acoustic nodes (LANs) for high-throughput fabrication of cell spheroids. Three orthogonal piezoelectric transducers (PZTs) were employed in this acoustic device to generate three orthogonal standing BAWs. We illustrated that these standing BAWs can create 3D dot-array (25 × 25 × 22) of LANs, through simulation and experiment validation. In this case, more than 13,000 aggregates were generated, and their number can be further increased by raising the position of the vertical PZT. To improve the maturation efficiency of cell aggregates into spheroids, we adopted GelMA hydrogels that can be rapidly photocured as supporting scaffolds to maintain and preserve the structure of cell aggregates after the withdrawal of acoustic fields or during the process of transferring them into Petri dish. As a result, most of cell aggregates (>90%) matured into cell spheroids with uniform size and high viability (>90%). Finally, we confirmed that these cell spheroids can be easily retrieved from the GelMA scaffold for subsequent drug testing.

2. Materials and methods

2.1. Acoustic device fabrication

To generate levitated acoustic nodes in three dimensions, three orthogonal acoustic standing waves are acquired, thus

the 3D acoustic assembly device was designed composed of three PZTs (PZT-41, Yantai Xingzhiwen Trading Co., Ltd.), a square acrylic chamber (21 × 21 × 10 mm), and a manual Z-axis moving apparatus (minimum step, 10 μm). The spacing between the two opposite walls of the chamber was an integer multiple of the half wavelength (λ = 500 μm). Two PZTs (20 × 10 mm; frequency, 3 MHz) were glued to the X and Y outer chamber with epoxy, respectively, and another PZT above the chamber was affixed to acrylic substrate (20 × 20 ×10 mm) that was mounted on the Z-axis moving apparatus (**Figure S1a** in Supplementary File). Each PZT was driven independently by a radio frequency (RF) signal generator (DG5352, Rigol) and a power amplifier (LCY-22 +, Minicircuit). To hold the cell suspension, a 1-mm thick acrylic sheet was glued to the chamber bottom.

2.2. Cell culture

Human hepatocellular carcinoma cell line C3A cells were cultured in Dulbecco's modified Eagle medium (Gibco) supplemented with 10% fetal bovine serum (Gibco) and 1% penicillin–streptomycin (Invitrogen, PA). The cells were cultivated in a humidified incubator at 5% CO_2 and 37°C in a T75 flask. At 80% confluence, cells were harvested with 0.25% trypsin-EDTA (Gibco) for sub-culture or cell suspension preparation.

2.3. Acoustic particle/cell assembly assay

The acoustic assembly device was placed on the fluorescence microscope stage, and a yellow light source was placed on the side of the acoustic device to supplement the upper bright light blocked by the vertical PZT, for observation of the assembly process. Then, fluorescent particles or fresh cell suspension (2 × 10^6 cells/mL) in 6% (w/v) GelMA (Regenovo) solution supplemented with 0.5% (w/v) lithium phenyl-2,4,6-trimethylbenzoylphosphinate (LAP) (Sigma-Aldrich) were introduced to the acoustic chamber. Before acoustic assembly assays, a ring-shaped polyimide heating film placed underneath the device was used to maintain the surrounding temperature around 37°C by a proportional-integral-derivative (PID) controller, in order to keep the GelMA's solution state. After that, the PZT located above the chamber slowly descended to the solution interface via *Z*-axis moving apparatus. To obtain good assembly pattern, the two PZTs in the horizontal direction were first applied with RF signals (frequency, 3.12 MHz, 3.10 MHz; 2–5 Vpp) to get a clear pattern of 2D array. Then, the vertical PZT was applied with another RF signal (2–5 Vpp) and the frequency of the signal (3.15 ± 0.2 MHz) was slowly adjusted until a periodical pattern of 3D dot-array appeared in the *Z* direction. Once particles or cells were assembled by desired patterns, the GelMA solution was crosslinked rapidly by a blue light (405 nm, 60 mW/cm^2, 30 s) to form a 3D hydrogel scaffold. Subsequently, the scaffold encapsulating particles or cell aggregates were transferred to a Petri dish (35 mm, Biosharp) for confocal imaging or culture, respectively. For the cell assembly culture, the hydrogel scaffold was further divided into smaller pieces (2 × 2 × 3 mm) using a sterile surgical blade to sustain the supply for oxygen and nutrients for encapsulated cells.

2.4. Spheroid retrieval

After 3 days of culture, cell aggregates were grown in the GelMA scaffold and mostly fused into spheroids. Then, these spheroids were released by dissociating the GelMA scaffold using GelMA lysis buffer (EFL-GM-LS-001, EFL) according to the kit instructions. The scaffold was washed with phosphate-buffered saline (PBS) three times and then incubated with GelMA lysis buffer at a ratio of 1:200 dilution with cell culture medium for 30 min at 5% CO_2 and 37°C. The spheroids were released, centrifuged, and resuspended, and then evenly transferred into an ultra-low attachment 96-well plate (Corning) with fresh cell culture medium in an incubator set at 37°C and 5% CO_2 for subsequent drug testing.

2.5. Cell viability assay

The cell viability was assessed with Live-Dead kit (Beyotime) following manufacturer's instructions. Briefly, cell aggregates in GelMA scaffold or cell spheroids in ultra-low attachment 96-well plate were washed with PBS thrice and then immersed in fresh Calcein-AM/propidium iodide (PI) staining solution (2 μM Calcein-AM and 4 μM PI in PBS). After 30 min of incubation at 5% CO_2 and 37°C, cell aggregates or spheroids were washed with PBS thrice and subsequently observed under a fluorescence microscope (Nikon, Ti-U, Japan). The cell viability was calculated as the ratio of the fluorescent area (green) to the total area using ImageJ software.

2.6. Drug testing

The retrieved C3A spheroids were tested for drug treatment using sorafenib, a targeted drug for advanced hepatocellular carcinoma, while the 2D culture was set up as control. To prepare the 2D culture, 2 × 10^4 cells were seeded in each well of a tissue culture-treated 96-well plate (Corning, 3916), while the retrieved spheroids were transferred to an ultra-low attachment 96-well plate (Corning, 3474). After 24 h of culture, both the spheroids and 2D cultures were treated with different concentrations of sorafenib solution (0, 0.1, 1, 5, 10, 25, 50 μM) in triplicate wells for 48 h of incubation at 5% CO_2 and 37°C. Then, the sorafenib solution was carefully removed, and fresh Calcein-AM/PI staining solution (2 μM Calcein-AM and 4 μM PI in PBS) was added to access cell viability.

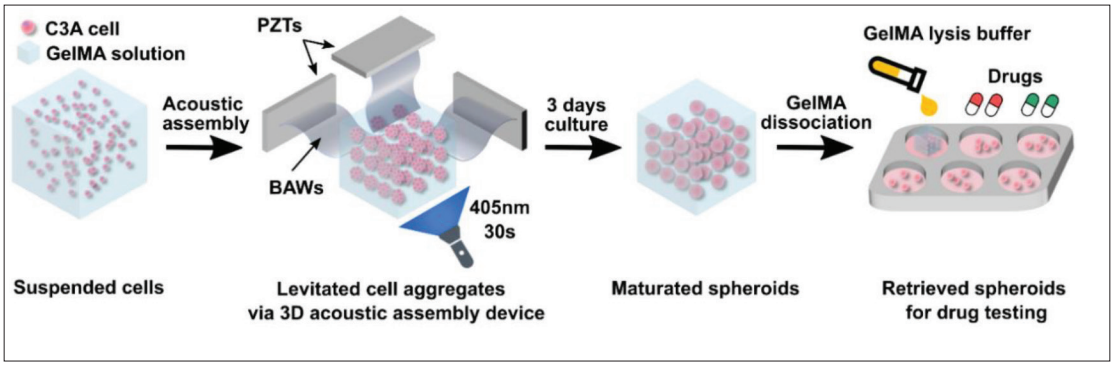

Figure 1. Working mechanism of the 3D acoustic assembly device for the high-throughput fabrication of cell spheroids. In 3D acoustic fields, the randomly suspended C3A cells in gelatin methacrylamide (GelMA) solution were acoustically levitated and assembled into cell aggregates with an 3D array pattern, once three orthogonal bulk acoustic waves (BAWs) generated by piezoelectric transducers (PZTs) were introduced. Then, blue light was turned on to photocrosslink the GelMA solution to maintain the structure of cell aggregates. After 3 days of culture, cell spheroids were formed and then retrieved for drug testing.

2.7. Numerical simulation

To simulate acoustic field in our MLANs device, a 3D finite element analysis (FEA) model was developed using COMSOL Multiphysics 5.4a. To reduce the computational amount, we only considered the fluidic domain. The three PZTs were considered plane wave radiation boundary conditions at the *X*, *Y*, *Z* sides of the fluidic domain (**Figure S1b** in Supplementary File). A frequency domain solver was used to calculate the 3D acoustic field.

2.8. Statistical analysis

All data presented are quantified from at least three independent experiments. All values are presented as mean ± standard error of the mean. Significant differences between experiment groups were evaluated by Student's *t*-test, and $P < 0.05$ was considered statistically significant.

3. Results and discussion

3.1. Device design and working principle

To improve the yield of spheroids using acoustic cell assembly devices, the presence of more acoustic nodes is a prerequisite for fabricating more spheroid. Here, we developed a 3D acoustic cell assembly device for high-throughput fabrication of cell spheroids (Figure 1). The device was made of three PZTs (20 × 10 mm; frequency, 3 MHz) located at the three orthogonal walls of the square chamber. After applying the RF signals, the PZTs excited three orthogonal BAWs that propagated into the bulk of the solution and coherently interfered with their own reflected waves from the opposed chamber wall to form three orthogonal standing BAWs. As a result, a 3D dot-array (25 × 25 × 22) of LANs was formed in the acoustic chamber. The number of LANs (>13,000) was higher than those obtained with currently used BAWs-based (>30) and SAWs-based (>12,000) acoustic devices[43,47], which meant that more cell aggregates could be fabricated by our acoustic devices. In this case, the suspended cells in GelMA solution were moved to the nearby LANs under the action of acoustic radiation force, and finally assembled into a 3D cell aggregate array. To facilitate the maturation of cell aggregates, aggregates need to be transferred into incubators. However, the process of transferring them will inevitably disrupt their aggregation structure, resulting in low maturation efficiency of spheroids[38]. To overcome this problem, we adopted biocompatible GelMA hydrogels that were photocured as supporting scaffolds[49], enabling to maintain and preserve the structure of cell aggregates. After that, the acoustic fields were withdrawn and these acoustically assembled cell aggregates within the GelMA hydrogel can be easily and non-disruptively transferred into Petri dishes for further incubation. During the 3 days of culture, most of cell aggregates (>90%) matured into cell spheroids, and were ready to be retrieved from the GelMA hydrogel dissociated by a GelMA lysis buffer for subsequent drug testing.

3.2. Characterization of 3D dot-array of LANs

In order to verify that the 3D dot-array of LANs was created, a numerical model was first used to predict the acoustic pressure field of the 3D acoustic assembly device (Figure 2a). The results showed that there are periodic distribution of levitated acoustic nodes in all three directions, as a result of a 3D dot-array of LANs created in the acoustic field. In general, suspended cells or particles are pushed toward the LANs under the action of acoustic radiation force (Figure 2b), and assembled into aggregates[42-44]. We used 10-μm fluorescent polystyrene particles to investigate it. To obtain good assembly pattern, the two PZTs in the horizontal direction were first applied with RF signals (frequency, 3.12 MHz, 3.10 MHz; 2–5 Vpp) to obtain a clear pattern of 2D array (**Videoclip S1**, with

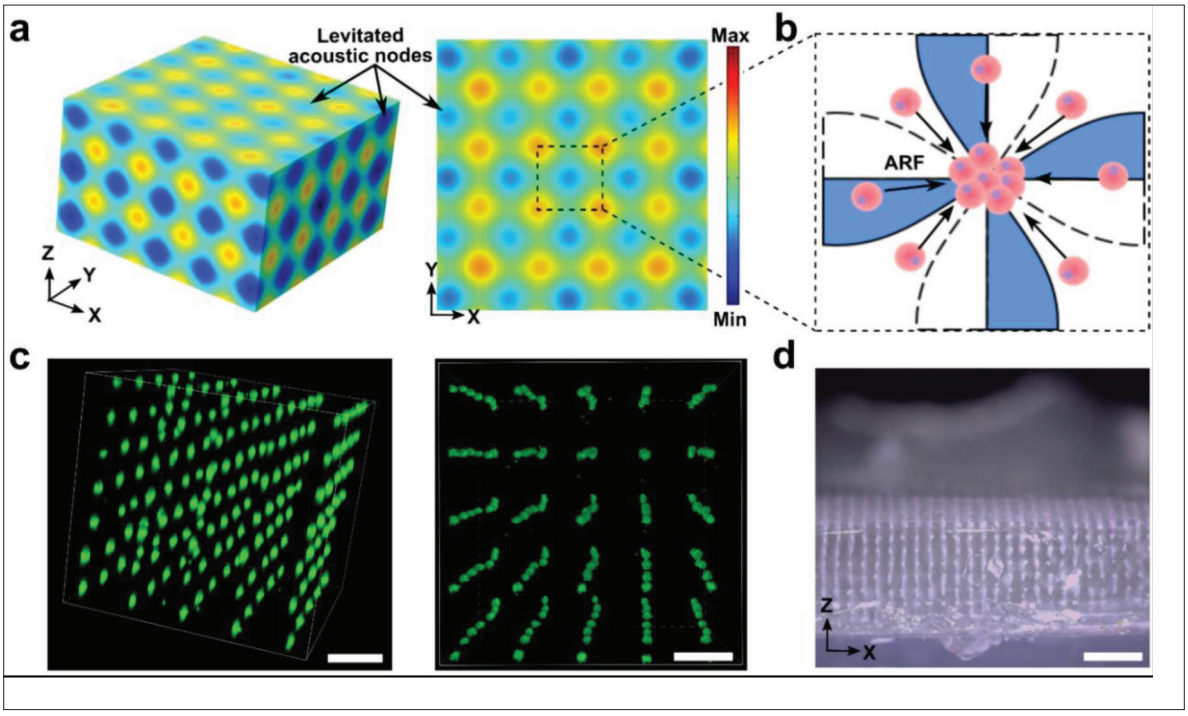

Figure 2. Characterization of the acoustic pressure field generated by the 3D acoustic assembly device. (a) Stereogram (left) and top view (right) of the simulated acoustic pressure field. The levitated acoustic nodes (minimal pressure) are periodically distributed in a 3D dot-array pattern. (b) In this acoustic field, the randomly suspended cells will move to the adjacent levitated acoustic nodes (LANs) under the action of acoustic radiation force (ARF). (c) 3D confocal images of the acoustically assembled particle aggregates. Scale bar: 250 μm. (d) Bright image of the particle aggregates periodically distributed in the gelatin methacrylamide (GelMA) hydrogel scaffold. Scale bar: 1 mm.

description in Supplementary File). Then, the vertical PZT was applied with another RF signal (2–5 Vpp) and the frequency of the signal (3.15 ± 0.2 MHz) was slowly modulated until the spherical aggregates alternately appeared and disappeared in the Z direction as the microscope's focus continued upward from the bottom (**Videoclip S2**, with description in Supplementary File). Subsequently, the GelMA solution was crosslinked by a blue light (405 nm, 60 mW/cm^2, 30 s) to fix the assembled particle aggregates. To visualize the location of aggregates within the GelMA hydrogel, a confocal microscopy was used. From the 3D confocal images (Figure 2c; **Videoclip S3**, with description in Supplementary File), the particle aggregates showed periodic distribution in both horizontal and vertical dimensions, forming a 3D dot-array pattern, which is consistent with our simulation result. Besides, the aggregates can be counted from the bright image as 25 × 25 × 9 = 5625 (Figure 2d).

3.3. High-throughput fabrication of aggregates

To obtain more cell spheroids, more LANs needed to be created in the acoustic device. Given that the standing BAWs present in the bulk of the solution, the number of LANs could be increased by adding more solution into the acoustic chamber; as a result, the height (H) of the solution was increased. In turn, the position of the vertical PZT was also elevated and positioned at the level of the solution. Theoretically, the number of created LANs can be estimated as 25 × 25 × L from Figure 2d. The L represented the layer of LANs in the Z direction, which was equal to $H/(\lambda/2)$, when H (mm) was an integer multiple of half wavelength (λ = 500 μm in this acoustic device, so that $L = 4H$)[39-41]. Thus, the more layers of LANs were created, the greater the total number of LANs. To verify it, we implemented an experiment: Suitable volume of GelMA solutions was repeatedly added into the acoustic chamber to form six H values (3, 3.5, 4, 4.5, 5, 5.5 mm). Then, the vertical PZT was exactly positioned at the level of the solution by a manual Z-axis moving apparatus (minimum step, 10 μm). Once particles were assembled by desired patterns, the GelMA solution was photocrosslinked rapidly to form a GelMA hydrogel within 30 s of blue light exposure, for all the liquids with the above-mentioned H values. To visualize the Z-direction distribution of aggregates, the GelMA hydrogel was placed side-down on a glass slide for the observation of an inverted microscope. Figure 3a shows that the aggregates have a good array pattern, and the numbers of the layered aggregates, by observation, are 12, 16, and 20, corresponding to H values of 3, 4, and 5 mm, respectively. Figure 3b shows that the layer of LANs was

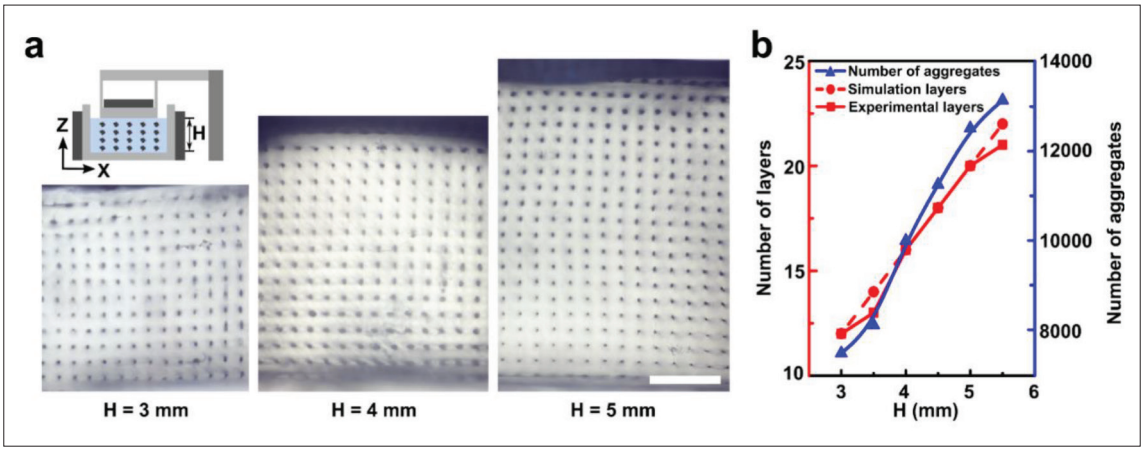

Figure 3. High-throughput fabrication of aggregates. (a) The number of aggregates fabricated by the 3D acoustic device were controllable with the adjustment on the height (*H*) of the solution. Scale bar: 1 mm. (b) Both the number of aggregate layer (*L*) and the yield show an increasing relationship with the *H*. In this acoustic device, more than 13,000 aggregates were fabricated.

linearly proportional to the *H*, having a good agreement with the simulation results. Accordingly, the total number of aggregates was also increased. At the *H* value of 5.5 mm, the number of aggregates was more than 13,000.

3.4. Acoustic assembly of cell spheroids

Having demonstrated the 3D acoustic assembly device's ability to produce high-throughput particle aggregates in a 3D-dot array pattern, we then applied them to fabricate cell spheroids. Hepatocellular carcinoma cell line, C3A cells, were evenly suspended in the 6% (w/v) GelMA solution (2×10^6/mL) containing 0.5% (w/v) LAP, and added into the acoustic chamber. The height of the solution was controlled at 3 mm. Once applying RF signals, a 3D-dot array of cell aggregates was generated, as shown in a serial view (**Videoclip S4**, with description in Supplementary File). It was observed that the acoustically assembled cell aggregates alternately appeared and disappeared as the microscope's focal layer continued to move upward from the bottom. Figure 4a shows the distribution of cell aggregates at three different layers. It clearly demonstrates that cell aggregates in each layer were arranged in a dot-array pattern, and had the same periodical distribution characteristic (Figure 4b). In this experimental setup, 7500 ($25 \times 25 \times 12$) cell aggregates were fabricated per operation.

To further mature the cell aggregates, these loosely formed aggregates need to be transferred into an incubator. However, the transfer process would inevitably disrupt their aggregation structure, resulting in low production efficiency and low yield of spheroids. To prevent that, we employed the GelMA material to constitute the cell suspension. It has two major characteristics: (i) rapid photopolymerization into a crosslinked hydrogel to maintain and protect the structure of acoustically assembled cell aggregates, and (2) superior biocompatibility to enable the growth and maturation of cells or cell aggregates[49,50]. In this experiment, once the cell aggregates were acoustically assembled, blue light was turned on for 30 s to initiate the photopolymerization of GelMA to form a hydrogel scaffold. Consequently, cell aggregates encapsulated in GelMA hydrogel can be easily and non-disruptively transferred into Petri dish supplemented with corresponding medium for a week and cultured in a humidified incubator. To sustain the supply of oxygen and nutrients for encapsulated cells, the GelMA hydrogel scaffold was divided into smaller pieces ($2 \times 2 \times 3$ mm). Figure 4c shows the dynamic growth of the cell aggregates within the GelMA scaffold. At day 1, these loosely assembled aggregates were still composed of individual cells. Interestingly, at day 3 they formed compact spheroids with smooth contours. At day 7, the spheroids further matured and become darker. We determined the formation efficiency of spheroid, which depends on the incubation time, by calculating the ratio of the number of compact spheroids to the total number of initial cell aggregates.

Figure 4d shows that the efficiency of spheroid formation had reached more than 90% at day 3. Furthermore, we tested the viability of cells during the acoustic assembly and culture process (Figure 4e and f). The results revealed good cell viability (>90%) and no significant difference as compared to cells without acoustic treatment. Together, these results demonstrated that the novel 3D acoustic assembly device enabled to fabricate cell spheroids in a high-efficiency, high-throughput, and low-cell damage manner.

3.5. Cell spheroid retrieval

To flexibly apply the cell spheroids for diverse biological studies, such as high-throughput drug screening and tissue engineering, the acoustically fabricated cell spheroids need

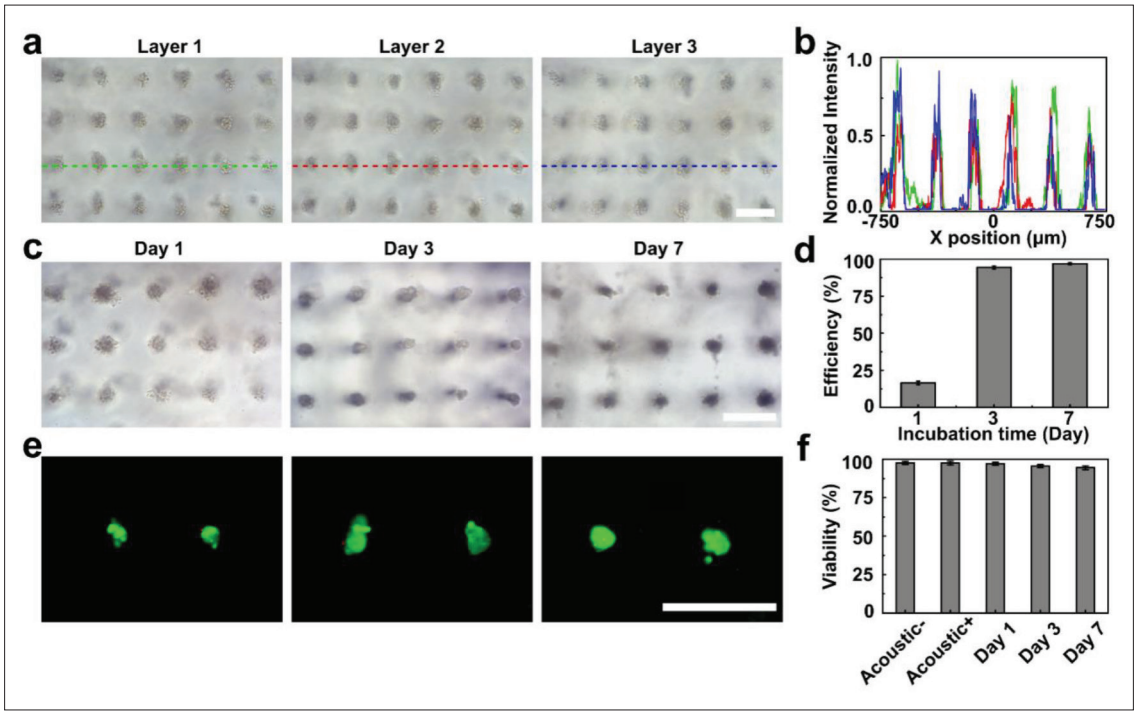

Figure 4. Cell spheroid fabricated by the 3D acoustic assembly devices. (a) Bright images of the acoustically assembled C3A cell aggregates at different layers. (b) The corresponding normalized line scan intensity curves at layer 1 (green), layer 2 (red), and layer 3 (blue). (c) The loosely assembled cell aggregates were gradually fused into compact cell spheroids during a 1-week culture. (d) The dependence of spheroid formation efficiency on incubation time. At day 3, the formation efficiency of cell spheroids was higher than 90%. (e) Live/dead staining and (f) viability assessment of the cell aggregates or spheroids during a 1-week culture. All scale bars: 250 μm each.

to be retrieved from the GelMA hydrogel scaffold. Here, we used a GelMA lysis buffer, which can dissociate the GelMA hydrogel to release the encapsulated spheroids. After a 3-day culture in incubator, the pieces of GelMA hydrogel were incubated with GelMA lysis buffer for 30 min. Figure 5a shows that hundreds of spheroids could be released. These retrieved C3A cell spheroids still retained their intact morphology and preserved specific albumin expression. The size distribution of the retrieved cell spheroids was further counted. In Figure 5b, the results showed that 80% of the spheroids were distributed in the size range of 90–120 μm. Furthermore, we observed the growth of cell spheroid after the dissociation treatment. The retrieved cell spheroids were transferred into a low-attachment culture plate for a 1-week culture. In Figure 5c, the results showed that the spheroid tended to be round and enlarged. Figure 5d shows the diameter of cell spheroids increased with the growth process. In addition, we evaluated the viability of cell spheroids by Calcein-AM/PI staining (Figure 5e). The retrieved spheroids remained viable (>90%) throughout the 1-week culture (Figure 5f). To conclude, we demonstrated that the acoustically fabricated spheroids can be easily retrieved from the GelMA hydrogel scaffold using GelMA lysis buffers, and the high cell viability remained, enabling them to be used as reliable and sufficient models for further studies, such as drug screening.

3.6. Drug testing

After obtaining a large number of spheroids using our 3D acoustic assembly devices, we further applied these acoustically fabricated spheroids in drug testing. As sorafenib is a first-line targeted drug for advanced liver carcinoma, we tested its efficacy against C3A spheroids[51,52]. The retrieved spheroids were dispensed into an ultra-low attachment 96-well plate and arranged into seven groups for six different drug concentrations (0.1, 1, 5, 10, 25, 50 μM) and control (vehicle only). Traditional 2D cell cultures were set as parallel experiments. After treatment with drug for 48 h, cell viability was measured using a live/dead staining assay. As shown in Figure 6a, dead cells appeared in the C3A spheroids at a drug concentration of 25 μM, while cell death in 2D cultures distinctly occurred at a drug concentration of 10 μM. The IC_{50} value was further calculated. Figure 6b shows that the IC50 value of spheroids (16.03 μM) was slightly higher than 2D cultures (13.52 μM), indicating higher drug resistance in spheroids, which could be attributed to several characteristics of 3D cultures[4-7]. In addition, the dead cell percentage increased rapidly in both 2D and spheroid cultures as the

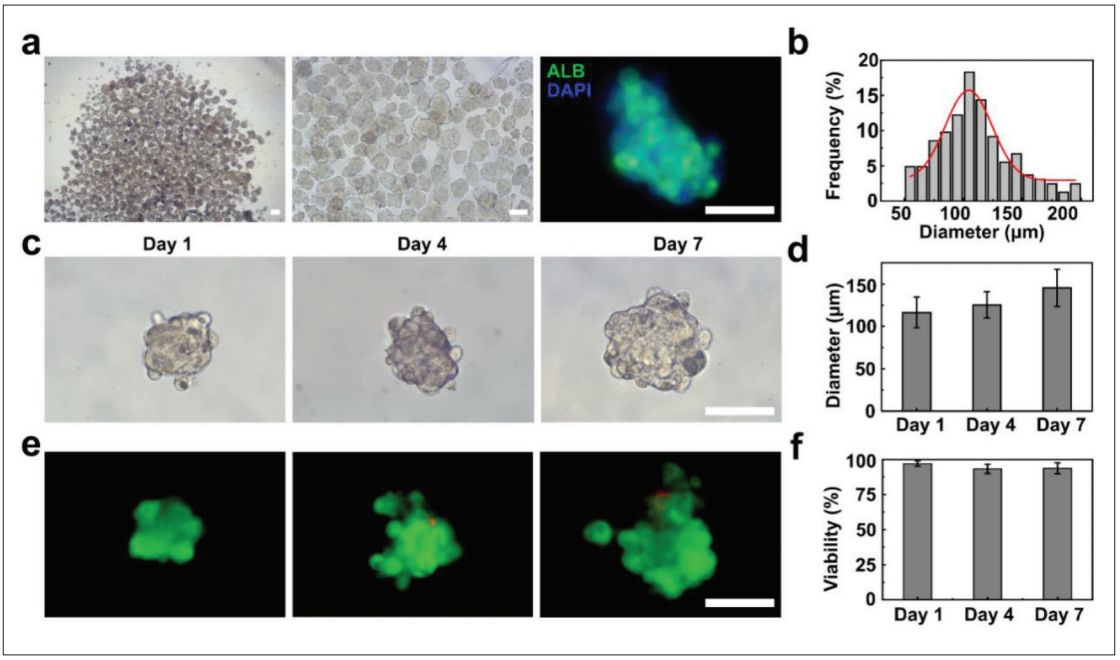

Figure 5. Retrieval of acoustically fabricated cell spheroids. (a) The first two bright images on the left show hundreds of spheroids released from the GelMA hydrogel scaffold, and the image on the right shows immunofluorescence staining for cell nuclei (DAPI, blue) and albumin (ALB, green) in the spheroid. (b) Spheroid size distribution. (c) Bright images of retrieved spheroid grown during a 1-week culture. (d) Bar chart of the spheroid diameter. (e) Live/dead staining and (f) viability assessment of the retrieved spheroids. All scale bars: 100 μm each.

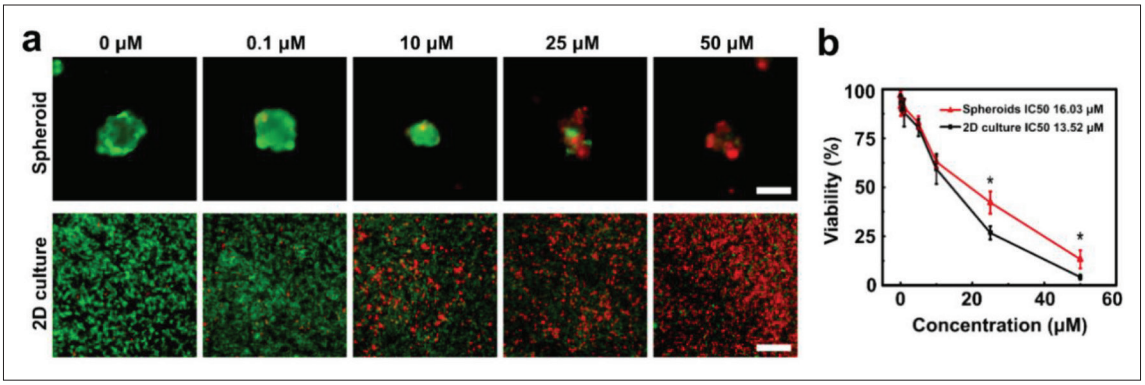

Figure 6. Anticancer target drug (sorafenib) testing on acoustically fabricated C3A spheroids. (a) Live/dead staining of C3A spheroids and 2D cultures after 48 h treatment with sorafenib. (b) The cell viability was measured. The statistical analysis showed significant differences between the spheroids and 2D cultures for different drug concentrations. *$P < 0.05$. Scale bar: 100 μm.

concentration of sorafenib increased, showing a dose-dependent response to the drug. Taken together, these results demonstrated that our acoustically fabricated spheroids can be used to evaluate drug efficacy and have great potential for high-throughput drug screening.

4. Conclusion

In this work, we presented the ability to improve the production yield of cell spheroids using our novel 3D acoustic assembly device. This device was capable of creating levitated acoustic nodes (LANs) in three directions, forming a 3D dot-array (25 × 25 × 22) of LANs. Based on this characteristic, a large number of cell aggregates arranged with the LANs were successfully assembled. To further improve the aggregate maturation, we adopted a 3D GelMA hydrogel scaffold strategy to maintain the structure of cell aggregates during the transfer process or incubation period. As a result, most cell aggregates (>90%) matured into spheroids that can be easily retrieved from the GelMA hydrogel in a non-destructive manner. The acoustically fabricated spheroids also manifested a higher

level of drug resistance than the traditional 2D cultures. We expect that the 3D acoustic cell assembly device will serve as a powerful tool for the scale-up fabrication of spheroids or even organoids for further biomedical applications, including as models for drug screening or as building blocks for tissue engineering and regenerative medicine.

Acknowledgments

The authors acknowledge the Confocal Microscope at the Institute of Basic Medicine and Cancer (IBMC), Chinese Academy of Sciences.

Funding

This work was supported by the National Key Research and Development Program of China (2022YFA1104600) and National Natural Science Foundation of China (31927801).

Conflict of interest

The authors declare no conflict of interest.

Author contributions

Conceptualization: Keke Chen
Data curation: Tingkuan Miao
Investigation: Tingkuan Miao, Beisi Huang, Yuecheng Qian
Resources: Ling Wang, Mingen Xu
Supervision: Mingen Xu
Writing – original draft: Keke Chen, Tingkuan Miao
Writing – review & editing: Keke Chen, Xiaoyun Wei

Ethics approval and consent to participate

Not applicable.

Consent for publication

Not applicable.

Availability of data

The data that support the findings of this work are available from the corresponding author, upon reasonable request.

References

1. Rodenhizer D, Dean T, D'Arcangelo E, *et al.*, 2018, The current landscape of 3D in vitro tumor models: What cancer hallmarks are accessible for drug discovery?. *Adv Healthc Mater*, 7(8):e1701174.

   https://doi.org/10.1002/adhm.201701174

2. Rodoplu D, Matahum JS, Hsu CH, 2022, A microfluidic hanging drop-based spheroid co-culture platform for probing tumor angiogenesis. *Lab Chip*, 22(7):1275–1285.

   https://doi.org/10.1039/d1lc01177d

3. Kim W, Gwon Y, Park S, *et al.*, 2023, Therapeutic strategies of three-dimensional stem cell spheroids and organoids for tissue repair and regeneration. *Bioact Mater*, 19:50–74.

   https://doi.org/10.1016/j.bioactmat.2022.03.039

4. Lin R, Chou L, Chien CM, *et al.*, 2006, Dynamic analysis of hepatoma spheroid formation: Roles of E-cadherin and beta1-integrin. *Cell Tissue Res*, 324(3):411–422.

   https://doi.org/10.1007/s00441-005-0148-2

5. Huang B, Wei X, Chen K, *et al.*, 2023, Bioprinting of hydrogel beads to engineer pancreatic tumor-stroma microtissues for drug screening. *Int J Bioprint*. 9(3):676.

   https://doi.org/10.1016/j.jconrel.2017.12.005

6. Li S, Yang K, Chen X, *et al.*, 2021, Simultaneous 2D and 3D cell culture array for multicellular geometry, drug discovery and tumor microenvironment reconstruction. *Biofabrication*, 13(4):045013.

   https://doi.org/10.1088/1758-5090/ac1ea8

7. Szűcs D, Fekete Z, Guba M, *et al.*, 2023, Toward better drug development: Threedimensional bioprinting in toxicological research. *Int J Bioprint*, 9(2):663.

   https://doi.org/10.18063/ijb.v9i2.663

8. Kim SJ, Kim EM, Yamamoto M, *et al.*, 2020, Engineering multi-cellular spheroids for tissue engineering and regenerative medicine. *Adv Healthc Mater*, 9(23):2000608.

   https://doi.org/10.1002/adhm.202000608

9. Banerjee D, Singh YP, Datta P, *et al.*, 2022, Strategies for 3D bioprinting of spheroids: A comprehensive review. *Biomaterials*, 291:121881.

   https://doi.org/10.1016/j.biomaterials.2022.121881

10. Zhuang P, Chiang YH, Fernanda MS, *et al.*, 2021, Using spheroids as building blocks towards 3D bioprinting of tumor microenvironment. *Int J Bioprint*, 7(4):444.

    http://doi.org/10.18063/ijb.v7i4.444

11. Skylar-Scott MA, Uzel SGM, Nam LL, *et al.*, 2019, Biomanufacturing of organ-specific tissues with high cellular density and embedded vascular channels. *Sci Adv*, 5(9):eaaw2459.

    https://doi.org/10.1126/sciadv.aaw2459

12. Ayan B, Heo DN, Zhang Z, *et al.*, 2020, Aspiration-assisted bioprinting for precise positioning of biologics. *Sci Adv*, 6(10):eaaw5111.

    https://doi.org/10.1126/sciadv.aaw5111

13. Chen K, Jiang E, Wei X, *et al.*, 2021, The acoustic droplet printing of functional tumor microenvironments. *Lab Chip*, 21(8):1604–1612.

    https://doi.org/10.1039/d1lc00003a

14. Daly AC, Davidson MD, Burdick JA, 2021, 3D bioprinting of high cell-density heterogeneous tissue models through spheroid fusion within self-healing hydrogels. *Nat Commun*, 12(1):753.

https://doi.org/10.1038/s41467-021-21029-2

15. Li L, Chen Y, Wang H, *et al.*, 2021, A high-throughput, open-space and reusable microfluidic chip for combinational drug screening on tumor spheroids. *Lab Chip*, 21(20):3924–3932.

https://doi.org/10.1039/d1lc00525a

16. Singh SK, Abbas S, Saxena AK, *et al.*, 2020, Critical role of three-dimensional tumorsphere size on experimental outcome. *BioTechniques*, 69(5):333–338.

https://doi.org/10.2144/btn-2020-0081

17. Pyo DH, Hong HK, Lee WY, *et al.*, 2020, Patient-derived cancer modeling for precision medicine in colorectal cancer: Beyond the cancer cell line. *Cancer Biol Ther*, 21(6):495–502.

https://doi.org/10.1080/15384047.2020.1738907

18. Brassard JA, Nikolaev M, Hubscher T, *et al.*, 2021, Recapitulating macro-scale tissue self-organization through organoid bioprinting. *Nat Mater*, 20(1):22–29.

https://doi.org/10.1038/s41563-020-00803-5

19. Han SJ, Kwon S, Kim KS, 2021, Challenges of applying multicellular tumor spheroids in preclinical phase. *Cancer Cell Int*, 21(1):152.

https://doi.org/10.1186/s12935-021-01853-8

20. Feng L, Liang S, Zhou Y, *et al*, 2020, Three-dimensional printing of hydrogel scaffolds with hierarchical structure for scalable stem cell culture. *ACS Biomater Sci Eng,* 6(5):2995–3004.

https://doi.org/10.1021/acsbiomaterials.9b01825

21. Shen H, Cai S, Wu C, *et al.*, 2021, Recent advances in three-dimensional multicellular spheroid culture and future development. *Micromachines*, 12(1):96.

https://doi.org/10.3390/mi12010096

22. Ryu NE, Lee SH, Park H, 2019, Spheroid culture system methods and applications for mesenchymal stem cells. *Cells*, 8(12):1620.

https://doi.org/10.3390/cells8121620

23. Rodrigues T, Kundu B, Silva-Correia J, *et al.*, 2018, Emerging tumor spheroids technologies for 3D in vitro cancer modeling. *Pharmacol Therapeut*, 184:201–211.

https://doi.org/10.1016/j.pharmthera.2017.10.018

24. Foty R, 2011, A simple hanging drop cell culture protocol for generation of 3D spheroids. *J Vis Exp*, 51:e2720.

https://doi.org/10.3791/2720

25. Tung YC, Hsiao AY, Allen SG, *et al.*, 2011, High-throughput 3D spheroid culture and drug testing using a 384 hanging drop array. *Analyst*, 136(3):473–478.

https://doi.org/10.1039/c0an00609b

26. He H, He Q, Xu F, *et al.*, 2019, Dynamic formation of cellular aggregates of chondrocytes and mesenchymal stem cells in spinner flask. *Cell Proliferat*, 52(4):e12587.

https://doi.org/10.1111/cpr.12587

27. Curcio E, Salerno S, Barbieri G, *et al.*, 2007, Mass transfer and metabolic reactions in hepatocyte spheroids cultured in rotating wall gas-permeable membrane system. *Biomaterials*, 28(36):5487–5497.

https://doi.org/10.1016/j.biomaterials.2007.08.033

28. Napolitano AP, Dean DM, Man AJ, *et al.*, 2007, Scaffold-free three-dimensional cell culture utilizing micromolded nonadhesive hydrogels. *BioTechniques*, 43(4):494, 496–500.

https://doi.org/10.2144/000112591

29. Wu Y, Zhou Y, Qin X, *et al.*, 2021, From cell spheroids to vascularized cancer organoids: Microfluidic tumor-on-a-chip models for preclinical drug evaluations. *Biomicrofluidics*, 15(6):061503.

https://doi.org/10.1063/5.0062697

30. Prince E, Kheiri S, Wang Y, *et al.*, 2022, Microfluidic arrays of breast tumor spheroids for drug screening and personalized cancer therapies. *Adv Healthc Mater*, 11(1):e2101085.

https://doi.org/10.1002/adhm.202101085

31. Yin F, Zhang X, Wang L, *et al.*, 2021, HiPSC-derived multi-organoids-on-chip system for safety assessment of antidepressant drugs. *Lab Chip*, 21(3):571–581.

https://doi.org/10.1039/d0lc00921k

32. Albrecht DR, Underhill GH, Wassermann TB, *et al.*, 2006, Probing the role of multicellular organization in three-dimensional microenvironments. *Nat Methods*, 3(5): 369–375.

https://doi.org/10.1038/nmeth873

33. Tocchio A, Durmus NG, Sridhar K, *et al.*, 2018, Magnetically guided self-assembly and coding of 3D living architectures. *Adv Mater*, 30(4):1705034.

https://doi.org/10.1002/adma.201705034

34. Parfenov VA, Koudan EV, Bulanova EA, *et al.*, 2018, Scaffold-free, label-free and nozzle-free biofabrication technology using magnetic levitational assembly. *Biofabrication*, 10(3):034104.

https://doi.org/10.1088/1758-5090/aac900

35. Souza GR, Molina JR, Raphael RM, *et al.*, 2010, Three-dimensional tissue culture based on magnetic cell levitation. *Nat Nanotechnol*, 5(4):291–296.

https://doi.org/10.1038/nnano.2010.23

36. Chen K, Wu M, Guo F, *et al.*, 2016, Rapid formation of size-controllable multicellular spheroids via 3D acoustic tweezers. *Lab Chip*, 16(14):2636–2643.

https://doi.org/10.1039/c6lc00444j

37. Olofsson K, Carannante V, Ohlin M, *et al.*, 2018, Acoustic formation of multicellular tumor spheroids enabling on-chip functional and structural imaging. *Lab Chip*, 18(16): 2466–2476.

https://doi.org/10.1039/c8lc00537k

38. Chen B, Wu Y, Ao Z, *et al.*, 2019, High-throughput acoustofluidic fabrication of tumor spheroids. *Lab Chip*, 19(10):1755–1763.

https://doi.org/10.1039/c9lc00135b

39. Armstrong JPK, Maynard SA, Pence IJ, *et al.*, 2019, Spatiotemporal quantification of acoustic cell patterning using Voronoï tessellation. *Lab Chip*, 19(4):562–573.

https://doi.org/10.1039/C8LC01108G

40. Bouyer C, Chen P, Guven S, *et al.*, 2016, A bio-acoustic levitational (BAL) assembly method for engineering of multilayered, 3D brain-like constructs, using human embryonic stem cell derived neuro-progenitors. *Adv Mater*, 28(1):161–167.

https://doi.org/10.1002/adma.201503916

41. Sriphutkiat Y, Kasetsirikul S, Zhou YF, 2018, Formation of cell spheroids using standing surface acoustic wave (SSAW). *Int J Bioprint*, 4(1):130.

http://dx.doi.org/10.18063/IJB.v4i1.130

42. Wu Z, Chen B, Wu Y, *et al.*, 2021, Scaffold-free generation of heterotypic cell spheroids using acoustofluidics. *Lab Chip*, 21(18):3498–3508.

https://doi.org/10.1039/d1lc00496d

43. Wu Y, Ao Z, Bin C, *et al.*, 2018, Acoustic assembly of cell spheroids in disposable capillaries. *Nanotechnology*, 29(50):504006.

https://doi.org/10.1088/1361-6528/aae4f1

44. Hu X, Zhao S, Luo Z, *et al.*, 2020, On-chip hydrogel arrays individually encapsulating acoustic formed multicellular aggregates for high throughput drug testing. *Lab Chip*, 20(12):2228–2236.

https://doi.org/10.1039/d0lc00255k

45. Chansoria P, Narayanan LK, Schuchard K, *et al.*, 2019, Ultrasound-assisted biofabrication and bioprinting of preferentially aligned three-dimensional cellular constructs. *Biofabrication*, 11:035015.

https://doi.org/10.1088/1758-5090/ab15cf

46. Wu Z, Jiang H, Zhang L, *et al.*, 2019, The acoustofluidic focusing and separation of rare tumor cells using transparent lithium niobate transducers. *Lab Chip*, 19(23): 3922–3930.

https://doi.org/10.1039/c9lc00874h

47. Jeger-Madiot N, Arakelian L, Setterblad N, *et al.*, 2021, Self-organization and culture of mesenchymal stem cell spheroids in acoustic levitation. *Sci Rep*, 11(1):8355.

https://doi.org/10.1038/s41598-021-87459-6

48. Cai H, Ao Z, Hu L, *et al.*, 2020, Acoustofluidic assembly of 3D neurospheroids to model Alzheimer's disease. *Analyst*, 145(19):6243–6253.

https://doi.org/10.1039/d0an01373k

49. Ying G, Jiang N, Yu C, *et al.*, 2018, Three-dimensional bioprinting of gelatin methacryloyl (GelMA). *Bio-Des Manuf*, 1(4):215–224.

https://doi.org/10.1007/s42242-018-0028-8

50. Wei X, Huang B, Chen K, *et al.*, 2022, Dot extrusion bioprinting of spatially controlled heterogenous tumor models. *Mater Design*, 223:111152.

https://doi.org/10.1016/j.matdes.2022.111152

51. Xu J, Ji L, Liang Y, *et al.*, 2020, CircRNA-SORE mediates sorafenib resistance in hepatocellular carcinoma by stabilizing YBX1. *Signal Transduct Tar*, 5:298.

https://doi.org/10.1038/s41392-020-00375-5

52. Nishikawa H, Nishijima N, Enomoto H, *et al.*, 2017, Prognostic significance of sarcopenia in patients with hepatocellular carcinoma undergoing sorafenib therapy. *Oncol Lett*, 14(2):1637–1647.

https://doi.org/10.3892/ol.2017.6287